JACC: CLINICAL ELECTROPHYSIOLOGY VOL. 12, NO. 2, 2026

ORIGINAL RESEARCH

BASIC SCIENCE

Inferior Sino-Atrial Node Exit Sites Are Associated With Electrical Remodeling

Jiahao Zheng, MSc,[a] Mathijs S. van Schie, PhD,[a] Lixia Dai, MD,[a] Paul Knops, BSc,[a] Jolanda Kluin, MD, PhD,[b] Yannick J.H.J. Taverne, MD, PhD,[b] Vadim V. Fedorov, PhD,[c] Natasja M.S. de Groot, MD, PhD[a,d]

ABSTRACT

BACKGROUND Electrical activity from the sino-atrial node (SAN) spreads via specific pathways into surrounding atrial tissue. Inferior sino-atrial node exit sites (SAN_i) have been observed in patients with structural heart disease and atrial fibrillation. However, determinants of preferential sino-atrial conduction pathways and the associated electrical properties of the SAN_i region remain poorly understood.

OBJECTIVES This study sought to examine differences in unipolar potential morphology and the degree of remodeling at the right atrium (RA) between patients with superior sino-atrial node exit sites (SAN_s) and SAN_i.

METHODS High-resolution epicardial mapping was performed in 27 patients with structural heart disease undergoing elective open-heart surgery. Electrodes within an 8-mm radius of the SAN exit site were classified as the SAN area. Electrophysiological properties, including potential voltage, conduction block, and R/S ratios, were computed.

RESULTS SAN_i, identified in 7 patients, exhibited lower potential voltages (median: 1.3 [Q1-Q3: 1.2-1.7] vs 2.6 [Q1-Q3: 2.2-3.6] mV; $P = 0.014$) and unipolar rS-wave morphologies, whereas SAN_s had full S-wave morphologies. The total activation times of RA were prolonged in SAN_i patients (median: 89 [Q1-Q3: 79-98] vs 78 [Q1-Q3: 66-85] milliseconds; $P = 0.046$). Heart rates were comparable between groups and remained consistent during both the preoperative and intraoperative periods.

CONCLUSIONS SAN_i identified by high-resolution epicardial mapping were associated with extensive RA remodeling and are most likely due to altered sino-atrial conduction pathways. (JACC Clin Electrophysiol. 2026;12:251-260)

The sino-atrial node (SAN) is the primary pacemaker of the heart and is generally located at the junction of the superior vena cava with the right atrium (RA).[1-3] However, other epicardial and endocardial locations of SAN impulse exit sites have been observed in both animal and human studies. Already in the late 1980s, Boineau et al[4] demonstrated in patients with Wolff-Parkinson-White syndrome that SAN exit sites were widely distributed in the RA. This could be explained by

From the [a]Department of Cardiology, Erasmus Medical Center, Rotterdam, the Netherlands; [b]Department of Cardiothoracic surgery, Erasmus Medical Center, Rotterdam, the Netherlands; [c]Bob and Corrine Frick Center for Heart Failure and Arrhythmia, The Ohio State University Wexner Medical Center, Columbus, Ohio, USA; and the [d]Department of Microelectronics, Signal Processing Systems, Faculty of Electrical Engineering, Mathematics and Computer Sciences, Delft University of Technology, Delft, the Netherlands.

The authors attest they are in compliance with human studies committees and animal welfare regulations of the authors' institutions and Food and Drug Administration guidelines, including patient consent where appropriate. For more information, visit the Author Center.

Manuscript received May 28, 2025; revised manuscript received September 9, 2025, accepted September 29, 2025.

ISSN 2405-500X https://doi.org/10.1016/j.jacep.2025.09.034

ABBREVIATIONS AND ACRONYMS

CB = conduction block
ECG = electrocardiography
EGM = electrogram
LVA = low-voltage area
RA = right atrium
SACP = sino-atrial conduction pathway
SAN = sino-atrial node
SAN_i = inferior SAN exit site
SAN_s = superior SAN exit site
SP = single potential
SR = sinus rhythm

either the existence of preferential sino-atrial conduction pathways (SACPs)[5-7] or supportive activation of subsidiary atrial pacemakers located inferiorly to the SAN pacemaker structure.[8,9]

Variable SAN exit sites can be due to functional and structural properties of atrial tissue. Overdrive pacing, often results in temporal caudal shifts of SAN exit sites, transitioning from superior to inferior locations.[10] However, at baseline sinus rhythm (SR), inferior SAN exit sites (SAN_i) have been found exclusively in patients with structural heart disease and a history of atrial fibrillation, suggesting that SAN_i are related to structural remodeling of atrial tissue.[11]

However, it remains unclear whether such remodeling alters SACPs, thereby contributing to shifts in SAN exit site. The aim of the current study is to therefore compare the degree of electrical remodeling at the RA between patients with superior SAN exit sites (SAN_s) and SAN_i.

METHODS

STUDY POPULATION. The study population consisted of 27 adult patients who underwent elective open-heart surgery in the Erasmus Medical Center Rotterdam, in whom a stable SAN exit site was observed in all consecutive beats during a SR recording of 5 seconds.

This study was approved by the Institutional Medical Ethical Committee (MEC2010-054/MEC2014-393), and written informed consent was obtained from all patients. Clinical data were extracted from electronic patient files. Preoperative surface electrocardiographs (ECGs) were used to characterize P-wave morphology, measure PR intervals, and determine sinus cycle length.

MAPPING PROCEDURE. Intraoperative epicardial high-resolution mapping during SR was performed with a multielectrode array containing 128 or 192 unipolar electrodes (interelectrode distances: 2 mm). The entire RA was sequentially mapped perpendicular to the terminal crest from the inferior to the superior caval vein. At each location, 5 seconds of SR were recorded. A pacemaker wire was stitched to the RA wall to record a temporal reference electrogram (EGM). All recorded data were stored on hard disk after amplification, filtering (bandwidth 0.5-400 Hz), sampling (1 KHz), and analog to digital conversion (16 bits).

DATA ANALYSIS. The surface ECG, the reference EGM, and all recorded unipolar EGMs were processed by custom-made software, which has previously been described in detail.[12] The steepest negative slopes of unipolar potentials were used to determine local activation times and construct activation maps.[13] Using the reference EGM, a total activation map of the entire RA was generated. In line with a prior series of studies, an interelectrode time difference larger than 12 milliseconds was defined as conduction block (CB), and potential voltages lower than 1 mV as low-voltage areas (LVAs).[14] Potentials were subdivided according to the number of deflections as single potentials (SPs) (1 single deflection), double potentials (2 deflections), and fractionated potentials (3 or more deflections). For each SP, the R/S ratio was calculated according to the relative R- and S-wave amplitude, which ranges from −1 to 1 (from a full R-wave to a full S-wave), as described previously.[15] P-wave durations and sinus cycle length from surface ECGs at lead II were measured and checked by 2 researchers.

IDENTIFICATION OF SAN ACTIVITY. The origin of the SAN activation was defined as the earliest activated area in the RA from which a focal activation pattern emerged as previously described.[16] Hence, the origin of this focal activation pattern had to be located at least 1 electrode away from the border of the mapping array. The origin of the SAN was assigned to either the most superior mapping location of the RA (SAN_s) or the remainder of the RA, including the mid- and inferior mapping locations (SAN_i). In all patients, a circle with a radius of 8 mm was around the SAN exit site, as shown in **Figure 1**. Electrophysiological properties within this SAN circle were compared between groups. The distance from the SAN exit site to the superior vena cava-RA junction was estimated by measuring the vertical distance from the SAN exit site to the most superior border of the electrode array at the uppermost location. Potential morphology at the SAN exit origin, was investigated within an area of 3 × 3 electrodes centralized on the first activated electrode.

STATISTICAL ANALYSIS. Continuous variables with an approximately normal distribution were expressed as mean ± SD and compared by Student's *t*-test, whereas skewed continuous variables were expressed as median (Q1-Q3) values and analyzed with Mann-Whitney *U* test. Categorical data were expressed as counts and percentages and analyzed

FIGURE 1 The Identification of Inferior and Superior SAN Exit Sites

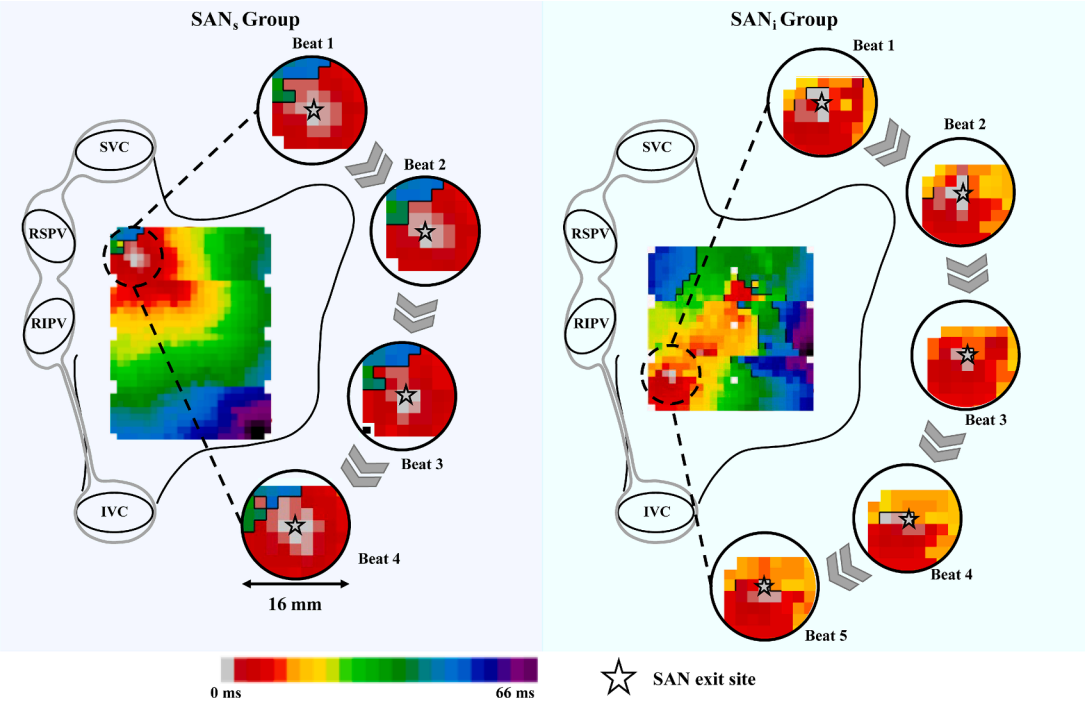

(Left) Example of a right atrial activation map of a patient with a superior sino-atrial node exit site (SAN$_s$). Based on the SAN exit site, all electrodes within an 8-mm radius around the SAN exit site were assigned to the SAN circle area. During 5 seconds, 4 sinus rhythm beats with stable exit sites were captured. (Right) Example of a right atrial activation map of a patient with an inferior sino-atrial node exit site (SAN$_i$); 5 consecutive sinus rhythm beats with stable exit sites are shown during 5 seconds of sinus rhythm. Black hollow star represents the SAN exit site; black lines indicate areas of conduction block; and gray lines indicate the terminal crest. IVC = inferior vena cava; RIPV = right inferior pulmonary vein; RSPV = right superior pulmonary vein; SAN = sino-atrial node; SVC = superior vena cava.

using Fisher exact test for 2 × 2 tables or the Fisher-Freeman-Halton exact test for larger contingency tables. Paired cycle lengths before vs during surgery were compared with the Wilcoxon matched-pairs signed-rank test. Comparisons of P-wave morphology, heart rate, SAN distance, and total activation time of the RA were performed with the Mann-Whitney *U* test. All other unpaired electrophysiological parameters underwent Mann-Whitney *U* testing followed by Benjamini-Hochberg false discovery rate correction for multiple comparisons. All tests were 2-tailed, and $P < 0.05$ was considered significant. Statistical tests were performed by IBM SPSS Statistics (version 28), GraphPad Prism (version 9.0, Dotmatics), and Python (version 3.8).

RESULTS

STUDY POPULATION. Of all 27 patients, 20 patients had a superior SAN exit site (SAN$_s$ group), and 7 patients had an inferior SAN exit site (SAN$_i$ group). Characteristics of both groups are listed in **Table 1**. Patients of the 2 groups did not differ in age (68 ± 8 vs 74 ± 10 years; $P = 0.187$), body mass index (27.8 ± 4.2 vs 30.5 ± 5.3 kg/m^2; $P = 0.244$). All patients in both groups demonstrated preserved left ventricular function. There were no significant differences in RA volume index (median: 20.3 [Q1-Q3: 14.5-25.3] vs 26.8 [Q1-Q3: 20.7-29.0] mL/m^2; $P = 0.234$) or LA volume index (median: 30.0 [1-Q3: 28.7-37.3] vs 35.9 [Q1-Q3: 26.9-44.4] mL/m^2; $P = 0.770$).

A total of 117,906 unipolar potentials (SAN$_i$: 3,974 ± 883 per patient, SAN$_s$: 4,504 ± 1,339 per patient; $P = 0.181$) recorded in 780 SR beats (SAN$_i$: 24 ± 8 per patient, SAN$_s$: 31 ± 14 per patient; $P = 0.211$) were analyzed. The SAN circle contained on average 344 ± 84 potentials covering 1.86 ± 0.24 cm^{2}per patient in the SAN$_i$ group and 359 ± 159 potentials ($P = 0.339$) covering 2.01 ± 0.30 cm^2 ($P = 0.245$) per patient in the SAN$_s$ group.

P-WAVE PROPERTIES. As illustrated in **Figure 2A**, PR intervals on the preoperative surface ECGs in the SAN$_i$ group were longer than the SAN$_s$ group

JACC: CLINICAL ELECTROPHYSIOLOGY VOL. 12, NO. 2, 2026
FEBRUARY 2026:251-260

TABLE 1 Patient Characteristics

	SAN_s (n = 20)	SAN_i (n = 7)	*P* Value
Male	16 (80)	6 (86)	>0.99
Age, y	68 ± 8	74 ± 10	0.187
BMI, kg/m^2	27.8 ± 4.2	30.5 ± 5.3	0.244
Hypertension	10 (50)	5 (71)	0.408
Dyslipidemia	9 (45)	1 (14)	0.204
Diabetes mellitus	4 (20)	3 (43)	0.328
Myocardial infarction	7 (35)	3 (43)	>0.99
RAVI,[a] mL/m^2	20.3 (14.5-25.3)	26.8 (20.7-29.0)	0.234
LAVI,[b] mL/m^2	30.0 (28.7-37.3)	35.9 (26.9-44.4)	0.770
Postoperation AF	10 (50)	4 (57)	>0.99
Underlying heart disease			0.858
IHD	9 (45)	4 (57)	
VHD	5 (25)	2 (29)	
I/VHD	6 (30)	1 (14)	
Antiarrhythmic agents			
Class I	0	0	
Class II	14 (70)	6 (86)	0.633
Class III	0	0	
Class IV	0	1 (14)	
History of AF			
Paroxysmal	0	1 (14)	
Persistent	0	0	
Long-standing persistent	0	0	

Values are n (%), mean ± SD, or median (Q1-Q3) unless otherwise indicated. The *P* values indicate significance between the total of the SAN_s group and the SAN_i group. [a]Available in 12 patients of SAN_s and 5 patients of SAN_i group. [b]Available in 12 patients of SAN_s and 4 patients of SAN_i group.

AF = atrial fibrillation; BMI = body mass index; IHD = ischemia heart disease; I/VHD = ischemia and valvular heart disease; LAVI = left atrium volume index; RAVI = right atrium volume index; SAN_i = inferior sino-atrial node exit; SAN_s = superior sino-atrial node exit; VHD = valvular heart disease.

(median: 209 [Q1-Q3: 198-225] vs 170 [Q1-Q3: 157-187] milliseconds; $P = 0.006$), whereas the heart rates were comparable between both groups (median: 62 [Q1-Q3: 57-75] vs 63 [Q1-Q3: 55-68] beats/min; $P = 0.386$). In addition, the P-wave durations in SAN_i patients were significantly longer than in SAN_s patients (median: 125 [Q1-Q3: 118-133] vs 100 [Q1-Q3: 92-111] milliseconds; $P < 0.001$). In both groups, sinus cycle length prior to surgery and during the mapping procedure were comparable (SAN_s: $P = 0.202$; SAN_i: $P = 0.469$) (Figure 2B).

ELECTRICAL PROPERTIES OF SAN EXIT SITES. Figure 1 shows an example of RA total activation maps of 1 patient from the SAN_s group and 1 patient from the SAN_i group, and the resulting RA activation pattern. In both patients, the SAN exit sites were consistently observed at their respective locations during the 5-second recording. The patient with SAN_i had a higher degree of conduction disorders throughout the RA and slower conduction within the SAN circle. In addition, there was a more superior expanding wave front that fused with the inferior wave front. As illustrated in Figure 2C, the distance from the SAN exit site to the superior vena cava-RA junction was significantly greater in SAN_i patients (median: 42 [Q1-Q3: 39-46] mm) compared to SAN_s patients (median: 8 [Q1-Q3: 4-11] mm; $P < 0.001$). Similarly, the total activation time of the entire RA was longer in SAN_i group (median: 89 [Q1-Q3: 79-98] milliseconds) than in the SAN_s group (median: 78 [Q1-Q3: 66-85] milliseconds; $P = 0.046$).

Typical examples of SAN circles and EGMs recorded at the SAN exit sites obtained from 2 patients from both groups are illustrated in Figure 3. In the patient with a SAN_s, unipolar potentials recorded consisted of large-amplitude, full S-wave potential. In contrast, unipolar potentials recorded from the patient with a SAN_i had lower amplitudes and consisted of an rS-wave morphology. As listed in Table 2, SPs recorded from the SAN_s consisted more frequently of a full S-wave morphology (median: 76.7% [Q1-Q3: 56.5%-91.0%] vs 9.7% [Q1-Q3: 2.0%-18.9%]; $P = 0.014$), whereas SPs recorded from the SAN_i consisted of a rS-wave morphology (median: 0.99 [Q1-Q3: 0.97-0.99] vs 0.84 [Q1-Q3: 0.75-0.88]; $P = 0.011$).

Comparing potential characteristics recorded from the SAN circles between the 2 groups, patients with a SAN_i had potentials with lower voltages (median: 1.3 [Q1-Q3: 1.2-1.7] vs 2.6 [Q1-Q3: 2.2-3.6] mV; $P = 0.014$) and more LVAs (median: 31.4% [Q1-Q3: 26.3%-40.3%] vs 10.4% [Q1-Q3: 5.0%-21.0%]; $P = 0.014$) compared to the SAN_s group (Figure 3B). The S-wave amplitudes of SPs in the SAN_i group were much lower compared with the S-wave amplitudes of SPs recorded from the SAN_s group (median: 1.4 [Q1-Q3: 1.0-1.7] vs 2.6 [Q1-Q3: 2.1-3.4] mV; $P = 0.022$), whereas the R waves were comparable (median: 0.1 [Q1-Q3: 0.0-0.1] vs 0.0 [Q1-Q3: 0.00-0.1] mV; $P = 0.434$). Furthermore, there were no differences observed between the 2 groups in terms of potential type (single-, double-, or fractionated potentials), SP duration (median: 76 [Q1-Q3: 70-80] vs 63 [Q1-Q3: 60-72] milliseconds; $P = 0.055$), or the amount of CB (SAN_i: median: 6.5% [Q1-Q3: 5.2%-14.4%] vs SAN_s: median: 8.6% [Q1-Q3: 4.8%-10.6%]; $P = 0.319$).

The upper panel of Figure 4 illustrates the size of areas activated within the first 20 milliseconds of atrial excitation in 2 patients with SAN_s or SAN_i. Compared to the SAN_s patients, these areas are smaller and more diffusely distributed in the SAN_i patients. Also, areas of CB are closely located to the earliest activated sites, resulting in multiple sites being activated approximately simultaneously. The lower panel shows the number of electrodes

FIGURE 2 Surface ECG Morphology and RA Mapping Parameters

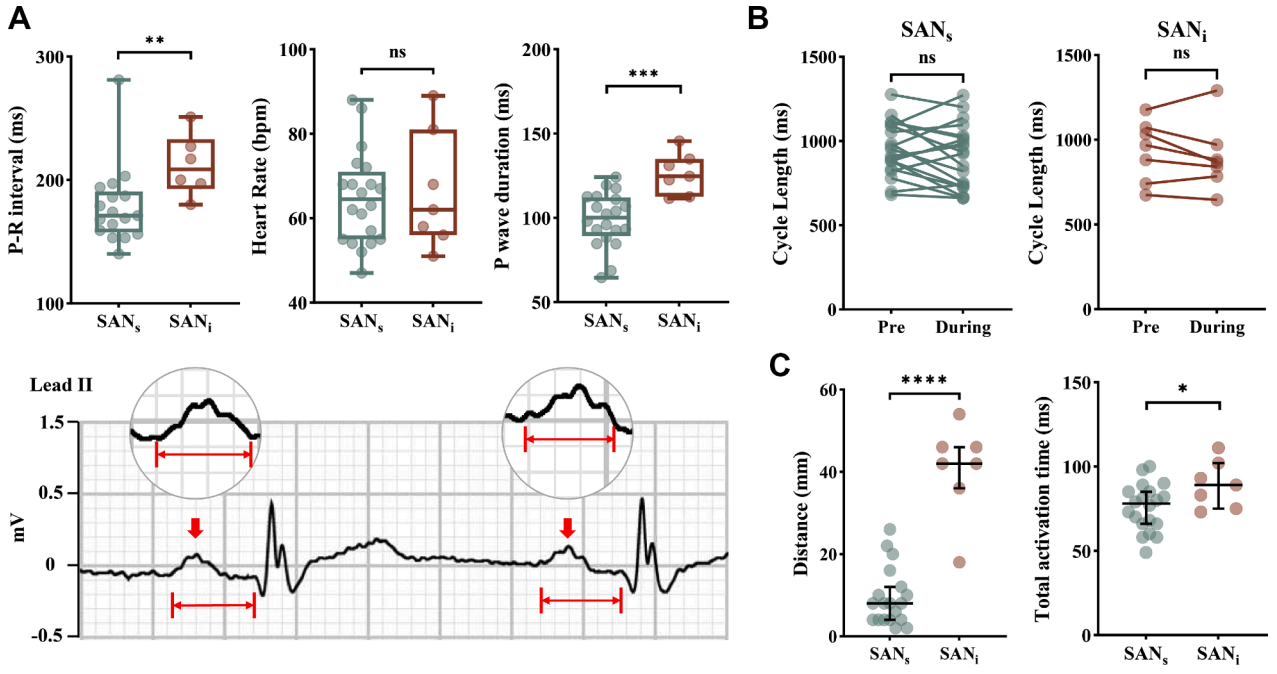

(A, upper) Box plots of the P-R interval, heart rate, and P-wave duration of the SAN_s and SAN_i groups separately; dots represent each individual patient. (A, lower) An example of 2 consecutive beats with prolonged P waves (>120 milliseconds) and P-R intervals (>200 milliseconds) in lead II, obtained from a SAN_i patient. (B) Comparison of sinus cycle length measured before and during the procedure in both groups. (C) Comparison of the distance from the SAN exit to the SVC–right atrial (RA) junction and the total RA activation time between the 2 groups. *$P < 0.05$; **$P < 0.01$; ***$P < 0.001$; ****$P < 0.0001$. ECG = electrocardiograph; NS = not significant; other abbreviations as in Figure 1.

activated within the first 20 milliseconds for all patients in 2 groups separately; from ≥5 milliseconds, the area activated in the SAN_s group is significantly larger than in the SAN_i group.

ELECTRICAL PROPERTIES OF THE SUPERIOR RA. Comparing the most superior mapping locations between the SAN_i and SAN_s patients, there were no differences in potential types, potential morphology, or the amount of CB (Table 3).

ELECTRICAL PROPERTIES OF THE ENTIRE RA. In the entire RA, SAN_i patients had considerably more LVAs (median: 9.9% [Q1-Q3: 8.7%-22.2%] vs 5.4% [Q1-Q3: 3.2%-8.7%]; $P = 0.037$) compared to SAN_s patients. Also, fewer SPs (median: 74.2% [Q1-Q3: 72.7%-77.8%] vs 84.4% [Q1-Q3: 78.0%-89.8%]; $P = 0.069$) were found in SAN_i patients at the expense of particularly double potentials (median: 22.1% [Q1-Q3: 20.6%-23.5%] vs 13.7% [Q1-Q3: 9.1%-17.8%]; $P = 0.044$). The 2 groups did not differ in the amount of CB ($P = 0.257$).

DISCUSSION

KEY FINDINGS. Compared to patients with a SAN_s, those with a SAN_i and stable SR exhibited prolonged P-wave and PR interval durations, lower potential voltages, more LVAs, and double potentials throughout the entire RA. These findings indicate more extensive RA remodeling. However, the presence of SAN_i was not associated with SAN bradycardia as SR cycle length before or during surgery, and electrophysiological properties at the most superior location of the RA were comparable between patient groups with superior and inferior SAN exit sites (Central Illustration). There are 2 possible explanations for this observation. First, the microarchitecture of the SAN head (superior compartment) itself could be damaged due to the presence of cardiovascular diseases and comorbidities. As such, there is more conduction impairment in the superior part of the SAN_i patients but it is not revealed due to the combination of nonuniform anisotropic tissue and reversal of the wave front

FIGURE 3 Electrophysiological Properties at SAN Exit Circles

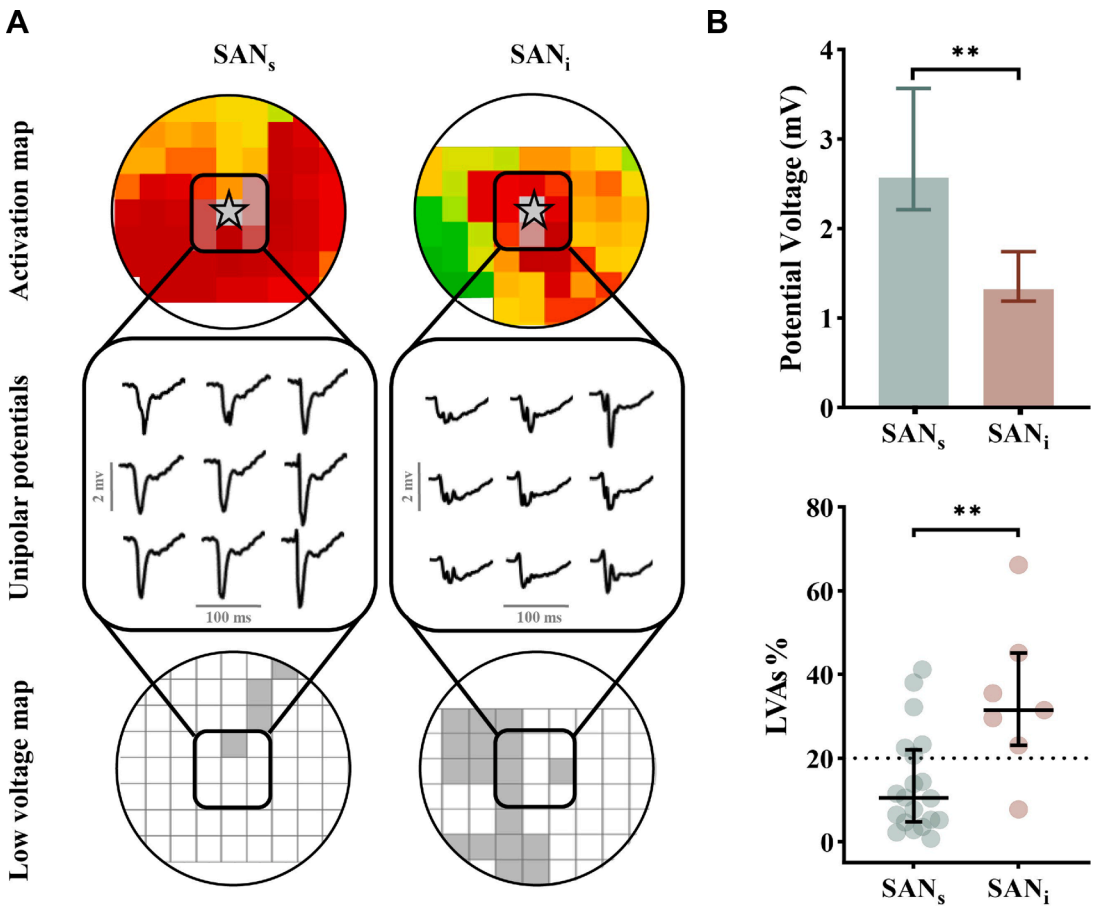

(A) Examples of an activation map containing SAN exit circles obtained from a SAN_s and a SAN_i patient. Corresponding unipolar potentials recorded from the center area of 3 × 3 electrode are depicted in the middle part and voltage maps demonstrating the spatial distribution of low voltage areas (LVAs) are depicted in the lower part. (B) Graphs demonstrating potential voltages and LVAs within the SAN circles for each patient within the SAN_s and SAN_i groups separately. $^{**}P < 0.01$. Abbreviations as in Figure 1.

propagation from a caudal to cranial direction compared to the SAN_s patients. Second, the SAN pacemaker structure becomes progressively more deeply embedded within the atrial wall from its superior (head) to inferior (tail) compartments (caudal-cranial axis), with only narrow pathways connecting it to the epicardial surface. Disease-induced CB may occur in these small pathways without being directly detectable on the epicardial surface.

INFERIOR SAN EXIT SITES. Li et al[6,7] provided compelling evidence for the existence of various alternative SACPs during prolonged SR cycle lengths induced by adenosine or tetrodotoxin. By stimulation of the vagal nerve in rabbits, Shibata et al[17] induced slowing of the heart rate accompanied by a shift in the dominant pacemaker location, which demonstrated the influence of the autonomic nervous system on the exit sites. SAN_i in humans have also been reported before.[17] Recently, Kharbanda et al[18] also reported changes in activation patterns at the superior RA in human during low-level vagal nerve stimulation via the tragus.

Sanders et al[19] observed a more caudal SAN exit site in a patient with SAN dysfunction and prolonged cycle length, which was attributed to structural remodeling of the RA. Other studies also demonstrated that patients with SAN dysfunction have a SAN_i, accompanied by P-wave prolongation and fractionation of EGMs.[20,21] Although our patients did not have sinus bradycardia and therefore no SAN dysfunction, patients with a SAN_i also had more fractionated potentials, low-voltage areas, and

P-wave prolongation among other things caused by decreased conduction velocity near the SAN exit sites. Despite the more extensive amount of conduction disorders, including slowing of conduction and CB in SAN_i patients, these phenomena mainly occur at the inferior RA rather than the superior RA. Importantly, no differences in SR cycle length were observed before or during surgery between patient groups with superior and inferior SAN exit sites.

Thus, inferior SAN exits during normal SR do not necessarily result from suppressed SAN automaticity or a pacemaker shift from the superior SAN primary pacemaker to an inferior, slower pacemaker within the SAN structure or a subsidiary atrial pacemaker. Instead, they may arise due to local conduction impairments of the superior SACPs, without evident SAN pacemaker dysfunction or pacemaker shifts.[6,7]

Ex vivo 3-dimensional imaging studies of the human SAN have identified up to 5 functional SACPs.[22] Due to intramural conduction from the SAN through the SACP to the atria, epicardial or endocardial exits can be located 5-25 mm away from the leading intranodal pacemaker. Notably, exit sites do not always correspond to the closest conduction pathway. SAN activation can exit inferiorly via inferior SACPs even when the leading pacemaker is in the SAN head, and vice versa.[6,23] Therefore, SAN_i should not be simply misinterpreted as an "inferior SAN," because no histological evidence in the published reports supports the existence of a distinct secondary "inferior" human SAN structure.[2,24-27] In this study, by directly mapping at the epicardium of the RA, we introduce new approaches and perspectives that may help further explore the potential mechanisms underlying SAN_i. Nevertheless, more histological and electrophysiological research is still needed to determine whether these phenomena arise from an alternative conduction pathway located inferiorly or from an inferior pacemaker.

TABLE 2 Electrophysiological Characteristics of the SAN Circle

	SAN_s	SAN_i	*P* Value
SAN exit sites			
SP with full S-wave, %	76.7 (56.5-91.0)	9.7 (2.0-18.9)	0.014
R/S ratio	0.99 (0.97-0.99)	0.84 (0.75-0.88)	0.011
SAN circle			
Voltage, mV	2.6 (2.2-3.6)	1.3 (1.2-1.7)	0.014
LVA, %	10.4 (5.0-21.0)	31.4 (26.3-40.3)	0.014
R-wave amplitude, mV	0.0 (0.00-0.1)	0.1 (0.0-0.1)	0.434
S-wave amplitude, mV	2.6 (2.1-3.4)	1.4 (1.0-1.7)	0.022
SP, %	68.7 (52.7-80.7)	70.3 (55.1-71.8)	0.434
DP, %	26.0 (17.6-35.5)	27.9 (26.3-37.5)	0.319
FP, %	4.7 (0.5-9.7)	4.5 (0.5-7.4)	0.434
SP duration, ms	63 (60-72)	76 (70-80)	0.055
Conduction block, %	8.6 (4.8-10.6)	6.5 (5.2-14.4)	0.319

Values are median (Q1-Q3). The *P* values indicate significance between the total of the SAN_s group and the SAN_i group.

DP = double potential; FP = fractionated potential; LVA = low voltage area; SAN = sino-atrial node; SP = single potential; other abbreviations as in Table 1.

UNIPOLAR POTENTIAL MORPHOLOGY AT THE EXIT SITES. Normal wave front propagation generates unipolar potentials consisting of a biphasic RS-wave morphology.[15] When an electrode is positioned at a site of initial activation (ie, the SAN or a subsidiary atrial pacemaker), the unipolar potential consists of a monophasic S-wave morphology as the depolarization wave front propagates away the recording site. A rS-wave morphology can thus be observed at a site where a "small" wave front first propagates toward the recording electrode after which a larger wave front propagates away from that site. In case this morphology is observed at a site containing a focal activation pattern, the r-wave morphology could be the result of a wave front originating from the SAN propagating in deeper layers within the atrial wall or a more inferiorly located exit site because the superior epicardial exit sites are inaccessible. In the present study, we demonstrated that potentials at both SAN exit sites may also contain R-waves with low amplitudes, suggesting that a small wave front is first propagating toward the exit sites site before spreading across the epicardium.

In a recent study, Kharbanda et al[28] demonstrated that patients with adult congenital heart disease more often had an rS-morphology at the SAN exit site, whereas pediatric patients with congenital heart disease more frequently had a full S-wave morphology. This difference could be explained by the fact that in adults the SAN is embedded deeper in the atrial wall with more fibrofatty tissue surrounding the SAN exit pathways. Despite the difference in R/S ratio between the SAN_i and SAN_s groups in our current study, the comparable size of the R waves indicate that in both groups a small wave front first propagates from deeper intramural layers toward the epicardial exit site. This pattern existed in patients from both groups, although the exit sites in the SAN_i group were located further from the physiological SAN.

STUDY LIMITATIONS. Intraoperative mapping was performed exclusively from the epicardial surface during cardiac surgery, and endocardial mapping data were not available in this patient group. Also, SAN tissue for histological analysis was not feasible due to the intraoperative setting. Additionally, detailed electrophysiological assessment of SAN function was not possible because of time

FIGURE 4 RA Excitation

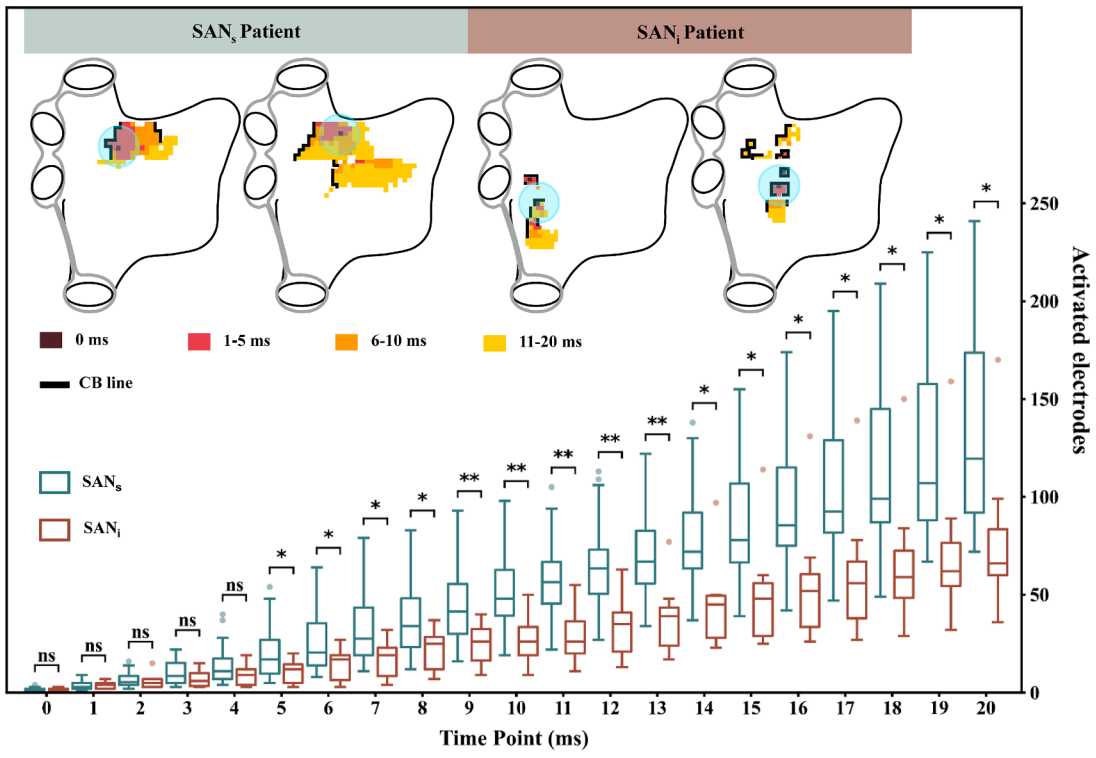

(Upper) Activation patterns during the initial 20 milliseconds of atrial excitation (colored areas) obtained from 2 patients with a SAN$_s$ or a SAN$_i$ exit site, including the spatial distribution of conduction block (CB) areas (thick black lines). The half transparent blue circles represent the SAN circle. (Lower) Graphs demonstrating the comparison of the number of activated electrodes per millisecond during the first 20 milliseconds between the 2 patient groups. *$P < 0.05$; **$P < 0.01$. Abbreviations as in Figures 1 and 2.

limitations, and the potential influence of general anesthesia on SAN exit site localization remains uncertain, although a standardized anesthesia protocol was used and exit sites remained consistent throughout mapping. The number of patients with SAN$_i$ was limited in this study, primarily because stable SAN$_i$ during baseline SR without pharmacological or neural stimulation are infrequently observed compared with SAN$_s$. Consequently, our conclusions must be interpreted with caution.

TABLE 3 Electrophysiological Characteristics at the Superior RA and Entire RA

	Superior RA (Include SAN Area)			Entire RA		
	SAN$_s$	SAN$_i$	*P* Value	SAN$_s$	SAN$_i$	*P* Value
Voltage, mV	3.5 (3.0-4.5)	4.0 (2.5-5.1)	0.415	4.6 (4.2-5.3)	3.2 (2.4-4.5)	0.064
LVA, %	9.6 (4.9-10.4)	16.8 (8.6-20.6)	0.415	5.4 (3.2-8.7)	9.9 (8.7-22.2)	0.037
R-wave amplitude, mV	0.9 (0.3-1.2)	1.2 (0.5-1.4)	0.415	1.4 (1.1-1.7)	0.6 (0.5-0.9)	0.037
S-wave amplitude, mV	3.4 (2.8-4.4)	3.6 (2.6-4.4)	0.445	3.8 (2.8-4.3)	2.6 (2.1-3.2)	0.048
R/S ratio	0.73 (0.69-0.79)	0.71 (0.63-0.75)	0.415	0.60 (0.54-0.64)	0.63 (0.59-0.69)	0.183
SP, %	75.1 (64.2-84.0)	71.3 (67.1-78.7)	0.445	84.4 (78.0-89.8)	74.2 (72.7-77.8)	0.069
DP, %	21.7 (13.3-29.7)	25.2 (19.7-27.8)	0.415	13.7 (9.1-17.8)	22.1 (20.6-23.5)	0.044
FP, %	3.2 (0.9-7.0)	2.7 (1.4-4.9)	0.415	1.5 (0.7-4.4)	3.5 (1.6-3.9)	0.262
SP duration, ms	53 (44-60)	57 (42-57)	0.456	56 (45-58)	51 (44-65)	0.423
Conduction block, %	4.9 (3.1-6.7)	4.2 (1.8-8.9)	0.445	3.7 (2.3-4.5)	5.0 (2.1-8.0)	0.257

Values are median (Q1-Q3) unless otherwise indicated. The *P* values indicate significance between the total of the SAN$_s$ group and the SAN$_i$ group.
RA = right atrium; other abbreviations as in Tables 1 and 2.

CENTRAL ILLUSTRATION **Comparison of Right Atrial Remodeling and Signal Morphology Between Patients With Superior and Inferior Sino-Atrial Node Exit Sites**

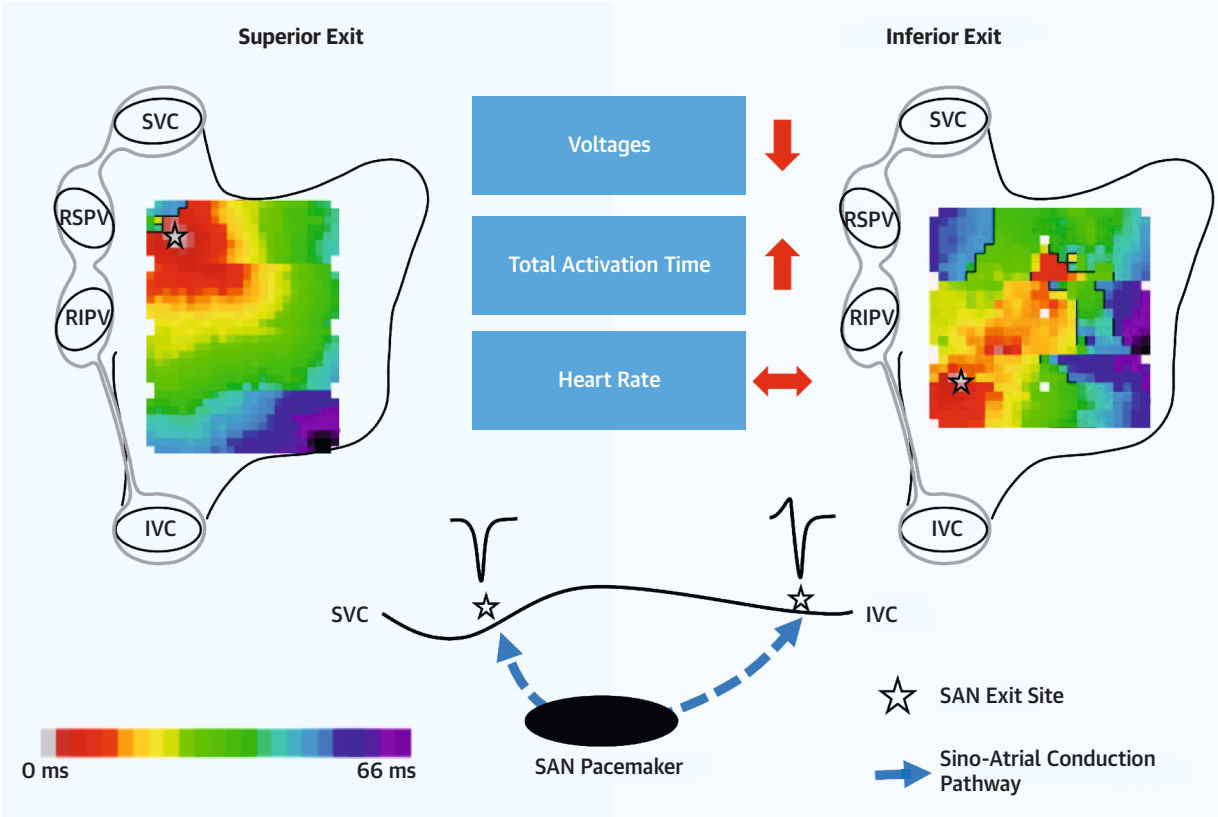

Zheng J, et al. JACC Clin Electrophysiol. 2026;12(2):251–260.

Upper left and right panels show right atrial activation maps from patients with superior and inferior SAN exit sites, respectively. The middle panel (text and schematic) indicates that patients with inferior SAN exit sites had lower unipolar potential voltages, longer total activation times, and smaller R/S ratios than those with superior exit sites, whereas heart rates were comparable. IVC = inferior vena cava; RIPV = right inferior pulmonary vein; RSPV = right superior pulmonary vein; SAN = sino-atrial node; SVC = superior vena cava.

Validation in larger, independent cohorts, ideally incorporating histological validation and 3-dimensional imaging mapping, will be essential to confirm these findings and clarify potential confounders.

CONCLUSIONS

SAN_i identified by high-resolution epicardial mapping were associated with extensive RA remodeling and are most likely due to altered sino-atrial conduction pathways, as suggested by the presence of normal heart rates and smaller R/S ratios at SAN_i areas compared to SAN_s areas.

ACKNOWLEDGMENTS The authors would like to kindly thank J.A. Bekkers, MD, PhD; W.J. van Leeuwen, MD; F.B.S. Oei, MD, PhD; P.C. van de Woestijne, MD; F.R.N. van Schaagen, MD; J. Sjatskig, MD; A. Khamooshian, MD; J.R.G. Etnel, MD, PhD; D.J. F.M. Thuijs, MD, PhD; W. Bakhuis, MD; and M.C. Roos-Serote, PhD, for their contribution to this work.

FUNDING SUPPORT AND AUTHOR DISCLOSURES

The authors have reported that they have no relationships relevant to the contents of this paper to disclose.

ADDRESS FOR CORRESPONDENCE: Prof Dr Natasja M.S. de Groot, Unit Translational Electrophysiology, Department of Cardiology, Erasmus Medical Center, Doctor Molewaterplein 40, 3015GD Rotterdam, the Netherlands. E-mail: n.m.s.degroot@erasmusmc.nl.

PERSPECTIVES

COMPETENCY IN MEDICAL KNOWLEDGE: Patients with RA remodeling who exhibited SAN_i nevertheless maintained normal heart rates. This finding suggests that SAN exit site variability may represent a functional adaptation rather than sinus node failure and should be taken into account during mapping and treatment of atrial arrhythmias.

TRANSLATIONAL OUTLOOK: Further studies combining endocardial mapping and tissue analysis are needed to validate the mechanisms underlying SAN exit shifts. The clinical impact of SAN_i on arrhythmia risk or treatment response remains to be established.

REFERENCES

1. Choudhury M, Boyett MR, Morris GM. Biology of the sinus node and its disease. *Arrhythm Electrophysiol Rev*. 2015;4(1):28–34.

2. Sánchez-Quintana D, Cabrera JA, Farré J, Climent V, Anderson RH, Ho SY. Sinus node revisited in the era of electroanatomical mapping and catheter ablation. *Heart*. 2005;91(2):189–194.

3. Boyett MR, Honjo H, Kodama I. The sinoatrial node, a heterogeneous pacemaker structure. *Cardiovasc Res*. 2000;47(4):658–687.

4. Boineau JP, Canavan TE, Schuessler RB, Cain ME, Corr PB, Cox JL. Demonstration of a widely distributed atrial pacemaker complex in the human heart. *Circulation*. 1988;77(6):1221–1237.

5. Fedorov VV, Schuessler RB, Hemphill M, et al. Structural and functional evidence for discrete exit pathways that connect the canine sinoatrial node and atria. *Circ Res*. 2009;104(7):915–923.

6. Li N, Hansen BJ, Csepe TA, et al. Redundant and diverse intranodal pacemakers and conduction pathways protect the human sinoatrial node from failure. *Sci Transl Med*. 2017;9(400):eaam5607.

7. Li N, Kalyanasundaram A, Hansen BJ, et al. Impaired neuronal sodium channels cause intranodal conduction failure and reentrant arrhythmias in human sinoatrial node. *Nat Commun*. 2020;11(1):512.

8. Rozanski GJ, Lipsius SL, Randall WC, Jones SB. Alterations in subsidiary pacemaker function after prolonged subsidiary pacemaker dominance in the canine right atrium. *J Am Coll Cardiol*. 1984;4(3):535–542.

9. Morris GM, D'Souza A, Dobrzynski H, et al. Characterization of a right atrial subsidiary pacemaker and acceleration of the pacing rate by HCN over-expression. *Cardiovasc Res*. 2013;100(1):160–169.

10. Parameswaran R, Lee G, Morris GM, et al. Simultaneous epicardial-endocardial mapping of the sinus node in humans with structural heart disease: impact of overdrive suppression on sinoatrial exits. *Heart Rhythm*. 2020;17(12):2154–2163.

11. Kharbanda RK, Wesselius FJ, van Schie MS, Taverne YJHJ, Boger ADJJC, de Groot NMS. Endo-epicardial mapping of in vivo human sinoatrial node activity. *JACC Clin Electrophysiol*. 2021;7(6):693–702.

12. Mouws EMPJ, Lanters EAH, Teuwen CP, et al. Impact of ischemic and valvular heart disease on atrial excitation: a high-resolution epicardial mapping study. *J Am Heart Assoc*. 2018;7(6):e008331.

13. de Groot NMS, Shah D, Boyle PM, et al. Critical appraisal of technologies to assess electrical activity during atrial fibrillation: a position paper from the European Heart Rhythm Association and European Society of Cardiology Working Group on eCardiology in collaboration with the Heart Rhythm Society, Asia Pacific Heart Rhythm Society, Latin American Heart Rhythm Society and Computing in Cardiology. *Europace*. 2022;24(2):313–330.

14. van Schie MS, Kharbanda RK, Houck CA, et al. Identification of low-voltage areas: a unipolar, bipolar, and omnipolar perspective. *Circ Arrhythm Electrophysiol*. 2021;14(7):e009912.

15. van Schie MS, Starreveld R, Roos-Serote MC, et al. Classification of sinus rhythm single potential morphology in patients with mitral valve disease. *Europace*. 2020;22(10):1509–1519.

16. Mouws EMJP, Lanters EAH, Teuwen CP, et al. Epicardial breakthrough waves during sinus rhythm: depiction of the arrhythmogenic substrate? *Circ Arrhythm Electrophysiol*. 2017;10(9):e005145.

17. Shibata N, Inada S, Mitsui K, et al. Pacemaker shift in the rabbit sinoatrial node in response to vagal nerve stimulation. *Exp Physiol*. 2001;86(2):177–184.

18. Kharbanda RK, Ramdat Misier NL, van Schie MS, et al. Insights into the effects of low level vagus nerve stimulation on atrial electrophysiology: towards patient tailored cardiac neuromodulation. *JACC Clin Electrophysiol*. 2023;9(9):1843–1853.

19. Sanders P, Morton JB, Kistler PM, et al. Electrophysiological and electroanatomic characterization of the atria in sinus node disease: evidence of diffuse atrial remodeling. *Circulation*. 2004;109(12):1514–1522.

20. Centurion OA, Isomoto S, Fukatani M, et al. Relationship between atrial conduction defects and fractionated atrial endocardial electrograms in patients with sick sinus syndrome. *Pacing Clin Electrophysiol*. 1993;16(10):2022–2033.

21. Joung B, Hwang HJ, Pak HN, et al. Abnormal response of superior sinoatrial node to sympathetic stimulation is a characteristic finding in patients with atrial fibrillation and symptomatic bradycardia. *Circ Arrhythm Electrophysiol*. 2011;4(6):799–807. https://doi.org/10.1161/circep.111.965897

22. Kalyanasundaram A, Li N, Augostini RS, Weiss R, Hummel JD, Fedorov VV. Three-dimensional functional anatomy of the human sinoatrial node for epicardial and endocardial mapping and ablation. *Heart Rhythm*. 2023;20(1):122–133.

23. Li N, Hansen BJ, Kennelly J, et al. High-resolution 3-dimensional multimodality imaging to resolve intramural human sinoatrial node pacemakers and epicardial-endocardial atrial exit sites. *Circ Arrhythm Electrophysiol*. 2023;16(4):e011528.

24. James TN. Anatomy of the human sinus node. *Anat Rec*. 1961;141:109–139.

25. Shiraishi I, Takamatsu T, Minamikawa T, Onouchi Z, Fujita S. Quantitative histological analysis of the human sinoatrial node during growth and aging. *Circulation*. 1992;85(6):2176–2184.

26. Chandler N, Aslanidi O, Buckley D, et al. Computer three-dimensional anatomical reconstruction of the human sinus node and a novel paranodal area. *Anat Rec (Hoboken)*. 2011;294(6):970–979.

27. Pambrun T, Derval N, Duchateau J, et al. Sinus node exit, crista terminalis conduction, interatrial connection, and wavefront collision: key features of human atrial activation in sinus rhythm. *Heart Rhythm*. 2022;19(5):701–709.

28. Kharbanda RK, van Schie MS, Ramdat Misier NL, et al. In-vivo sino-atrial node mapping in children and adults with congenital heart disease. *Front Pediatr*. 2022;10:896825.

KEY WORDS electrophysiology, epicardium mapping, right atrium remodeling, sino-atrial conduction pathway, sino-atrial node